Structural Design and Characterization of $BaMg_xCo_{2-x}Fe_{16}O_{27}$ Hexaferrites Based on *ab initio* Computations

M. Bakhtiari[a], G. Nabiyouni[a,*] and A. Besharati-Seidani[b]

[a]Department of Physics, Faculty of Science, Arak University, Arak 3815688943, Iran

[b]Department of Chemistry, Malek Ashtar University of Technology, Tehran, Iran

(Received February 7, 2014; in final form November 7, 2014)

Structural design of barium hexaferrites $BaMg_xCo_{2-x}Fe_{16}O_{27}$ (x = 0.0, 1, 2) has been studied, and the magnetic and electronic structure of that has then been investigated using first principle total energy calculation. All calculations are based on the density functional theory. In order to improve the description of strongly correlated $3d$ electrons of iron, the general gradient approximation plus Hubbard U (GGA+U) method is used. We found that in the lowest energy configuration Mg and Co ions preferentially occupy the 6g sites. With the increase of Mg content x, the energy gap of $BaMg_xCo_{2-x}Fe_{16}O_{27}$ increases but the lattice constant of unit cell decreases. The magnetic moment of the unit cell for Mg content x = 0, 1, and 2 are calculated to be 52, 49 and 46 μ_B/cell, respectively, in agreement with previous experimental results. The substitutions of Mg and Co at the $BaFe_2^{2+}Fe_{16}^{3+}O_{27}$ decrease electrical conductivity and transit it from a half-metal to semiconductor material. Based on our calculations on electronic band structure, the $BaFe_2Fe_{16}O_{27}$ (BFFO) is a weak half-metal, but $BaMg_2Fe_{16}O_{27}$ (BMFO), $BaMgCoFe_{16}O_{27}$ (BMCFO) and $BaCo_2Fe_{16}O_{27}$ (BCFO) are semiconductors. The electrical resistivity increases by increasing Mg and Co contents due to increase in porosity which prevents the hopping of charge carriers.

DOI: 10.12693/APhysPolA.126.1288

PACS: 75.50.Gg, 71.20.–b, 75.75.–c, 71.15.Mb, 71.15.Dx

1. Introduction

In the last decades, ferrite magnetic materials have been considered as important electromagnetic wave absorbing materials with interesting magnetic properties because their electric and magnetic properties are suitable for absorbing the ultra-high frequency band [1]. With the arrival of modern electronic, microwave and magnetic devices, the electromagnetic interference has become a critical problem [2]. It is therefore important to design materials that can attenuate electromagnetic radiations. Wave absorbing materials are required to have a large electric and magnetic loss in the frequency range of interest.

Polycrystalline hexagonal ferrites are technologically desirable materials due to their high resistivity and high permeability make them suitable for various applications. Barium hexagonal ferrites (BHF) are ideal filters for electromagnetic interference attenuation purposes due to their low cost, high stability and high density [3]. The crystal structure of barium hexagonal ferrites (BHF) are divided into six different types: M ($BaFe_{12}O_{19}$), W ($BaMe_2Fe_{16}O_{27}$), Y ($Ba_2Me_2Fe_{12}O_{22}$), Z ($Ba_3Me_2Fe_{24}O_{41}$), X ($Ba_2Me_2Fe_{28}O_{46}$) and U ($Ba_4Me_2Fe_{36}O_{60}$), where Me is Mg or any divalent transition metal such as Mn, Fe, Co, Ni, Cu, and Zn. The electrical conductivity and dielectric behavior of these materials depend on many factors such as preparation method, sintering temperature and type of substitutes [4].

In the series of barium hexagonal ferrites, the W-type Ba-hexaferrites have high magnetic permeability due to their high values of saturation magnetization and exhibiting excellent magnetic anisotropy. Thus compared to the other coordination hexagonal ferrites, their microwave absorption characteristics have potential applications in magnetic and microwave devices [5]. The crystal structure of W-type hexagonal ferrites can be depicted as an alternating staking of S and R blocks in the direction of hexagonal c-axis and the general formula of this type is SSR*S*S*R, where the S (spinel block) is a two-oxygen layer block with the formula of $Fe_6O_8^{2+}$ and R is a three-oxygen layer block with the formula of $BaFe_6O_{11}^{2-}$. There is a 180 degree rotation about the c axis between S, S* and R, R* [6, 7].

Substitution of Ba^{2+}, Me^{2+} or Fe^{3+} ions is an effective method to vary the magnetic properties such as the saturation magnetization [8]. The presence of divalent and trivalent cations distributed among various sublattices makes the W-type haxaferrite very interesting for basic studies and different technical applications [4]. Several research groups have studied the structural, magnetic and electrical properties of the Ba hexaferrite from the first principles [9–12].

In the present work, the structure and the magnetic properties of the W-type barium hexaferrite $BaMg_{2-x}Co_xFe_{16}O_{27}$ (x = 0.0, 1, 2) were studied using first principle method. The electronic ground structure was also investigated.

*corresponding author; e-mail: g-nabiyouni@araku.ac.ir

2. Calculations details

We have used the *ab initio* calculations using the plane-wave ultrasoft pseudopotential scheme within the spin density functional theory (DFT) [13] in the framework of generalized gradient approximation plus Hubbard U (GGA+U). Each cation (i.e., Mg, Co, Fe) should have different effective U values. With varying U parameters, even the qualitative behavior of the band dispersion as well as the magnetic ordering can be changed. The ultrasoft pseudopotentials have been used for $3s$, $3p$, $3d$, $4s$, and $4p$ states of Fe atoms, $3d$, and $4s$ states of Co atoms, $3s$ state of Mg atoms and $2s$, and $2p$ states of O atoms in valence configurations, respectively [14].

Generalized gradient approximation functional in the form of Perdew–Burke–Ernzerhof (PBE) [15] was used for the electronic exchange-correlation potentials in the DFT calculations. GGA is expected to be more accurate than local density approximation (LDA) for our calculations.

The ultrasoft pseudopotentials and the exchange-correlation energy are used to represent the interaction between ionic cores and valence electrons. The total energy and electronic structure are determined by solving the Kohn–Sham equations [16, 17] via the iterative matrix diagonalization scheme based on the Davidson method. The whole set of self-consistent calculations is performed using the plane wave PWSCF code in the QUANTUM-ESPRESSO package [18], which is based on the DFT. The Kohn–Sham single-particle electron wave functions were expanded in a basis of plane-waves set up to a cut-off kinetic energy (E_{cutoff}) of 40 Ry for all structures, and the energy cutoff for the charge density was 320 Ry that are sufficient to get well converged results.

The number of sampling k-points used in the Brillouin zone (BZ) summation of the electronic density and total energy is increased until the total energy converges to 0.0001 Ry. The irreducible BZ investigations are carried out using the scheme of the Monkhorst–Pack [19] with the $8 \times 8 \times 2$k point mesh. The relaxed internal atomic positions have been obtained by total-energy and atomic-force minimization using the Hellmann–Feynman theorem. For the force convergence, all atom coordinates and lattice vectors are fully relaxed until the Hellmann–Feynman forces acting on each atom were less than 0.001 Ry/a.u. All calculations are spin-polarized with atom spin configuration initialized according to Gorter scheme [20].

3. Result and discussion

The crystal unit cell of W-type barium hexaferrite $BaFe_2^{2+}Fe_{16}^{3+}O_{27}$ contains two formula units i.e. 92 atoms. As shown in Fig. 1, the oxygen atoms are close packed with the Ba and Fe ions in the interstitial sites. The structure is built up from smaller units: four cubic blocks S, having the spinel-type structure, and two hexagonal blocks R, contain Ba ions. Therefore, the unit cell is composed of the sequence RSSR*S*S*. Fe^{3+} ions

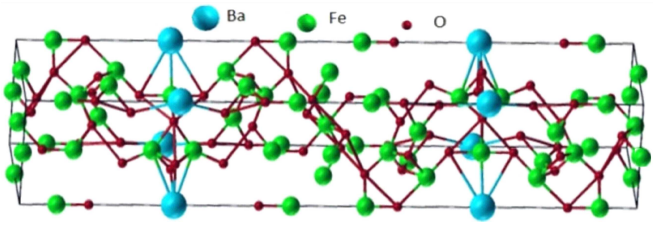

Fig. 1. Crystal structure of BFFO contains two formula units i.e. 92 atoms.

allocated in five distinctive sublattices, namely 2a, 2b, $4f_1$, $4f_2$ and 12k, which are distributed in both blocks. Three of these positions, 2a, $4f_2$ and 12k have octahedral site, while $4f_1$ shows tetrahedral site and 2b occupies a pseudotetrahedral site. Furthermore, $4f_1$ and $4f_2$ sites have spin down configurations, while other three sites contribute positively to magnetization [3]. On the other hand, the Fe^{2+} ions are positioned at seven crystallography different sites, namely 2d, $4f_1$ ($4f^{VI}$R), $4f_2$ ($4f^{IV}$), $4f_3$ ($4f^{VI}$S), 6g, 4e and 12k. As shown in Table I, three of these positions, i.e. 4e, $4f_1$ and $4f_2$ sites, have spin down configurations, while the configuration of the other four sites, 2d, $4f_3$, 6g and 12k have spin up.

TABLE I

Coordinates of Fe^{2+} atoms for barium hexaferrite $BaFe_2^{2+}Fe_{16}^{3+}O_{27}$ with space group of $P63/mmc$.

Atom	Wyckoff site	Coordination	Spin	Block	Coordinates		
					x	y	z
$Fe^{2+}(1)$	2d	pseudotetra	↑	R	1/3	2/3	3/4
$Fe^{2+}(2)$	$4f_1$	octahedral	↓	R	1/3	2/3	0.208
$Fe^{2+}(3)$	$4f_2$	tetrahedral	↓	S	1/3	2/3	0.092
$Fe^{2+}(4)$	4e	tetrahedral	↓	S	0	0	0.055
$Fe^{2+}(5)$	$4f_3$	octahedral	↑	S	1/3	2/3	0.575
$Fe^{2+}(6)$	6g	octahedral	↑	S–S	1/2	0	0
$Fe^{2+}(7)$	12k	octahedral	↑	R–S	5/6	2/3	0.14

Because of fractional population parameters of Mg and Co locations, several models for Mg and Co locations were used. Depending on the material preparation conditions, the populations of Mg cations located in symmetric sites of the cell are somewhat different and the Mg^{2+} ions have a statistical distribution over tetrahedral and octahedral sites, but mainly prefer to locate at the octahedral sites. The Mg cations of $BaMg_2Fe_{16}O_2$ (BMFO) are mainly distributed in the 6g and $4f_3$ sites [21]. Also, the populations of Co cations located in symmetric sites of the $BaCo_2Fe_{16}O_{27}$ (BCFO) cell are mainly distributed in the 6g sites (octahedral sites S–S and S*–S* interface) and $4f_3$ octahedral sites of S blocks [22]. For simplicity two structural arrangement of BMFO and two structural arrangement of BCFO were proposed as follows:

Arrangement I: all of the four Mg cations of the unit cell are assumed to be located at 2/3 positions among six positions of 6g sites (Fig. 2a).

Arrangement II: all of the four Mg cations of the unit cell are assumed to be located at all four positions

of $4f_3$ sites (Fig. 2b).

Arrangement III: all of the four Co cations of the unit cell are assumed to be located at 2/3 positions among six positions of 6g sites (Fig. 2c).

Arrangement IV: all of the four Co cations of the unit cell are assumed to be located at all four positions of octahedral $4f_3$ sites (Fig. 2d).

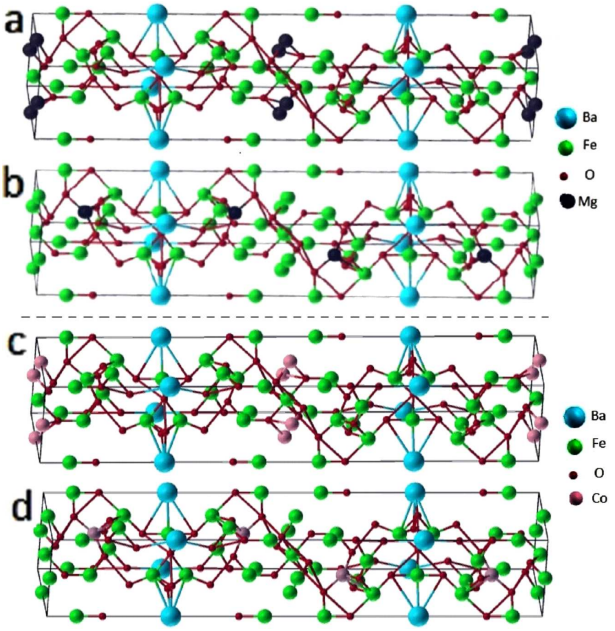

Fig. 2. Crystal structure of (a) model I of BMFO, (b) model II of BMFO, (c) model III of BCFO, (d) model IV of BCFO. Located in interface of S–S or S*–S* is 6g sites of Fe.

The initial lattice parameters and detailed ion coordinates of $BaFe_2Fe_{16}O_{27}$ (BFFO) and $BaMg_2Fe_{16}O_{27}$ (BMFO) and $BaCo_2Fe_{16}O_{27}$ (BCFO) were accepted from previous experimental works [20, 22, 23]. Measured lattice parameters and magnetic moments of BFFO are $a = 5.88$ Å, $c = 32.845$ Å, $c/a = 5.586$ and 56 μ_B/cell. Calculation of the BFFO initial cell gives the optimized lattice parameters of: $a = 5.941$ Å, $c = 33.30$ Å, $c/a = 5.605$ and the magnetic moment of 56 μ_B/cell.

The optimized lattice parameters and free energies for BMFO and BCFO calculated using four arrangements are shown in Tables II and III, respectively. Although the symmetry of arrangement I and arrangement III are lower than that of arrangement II and arrangement IV, the structure of Arrangement I is more stable than that of Arrangement II, because there is about –0.3 eV/cell of the free energy differences between them. The structure of Arrangement III is also more stable than that of Arrangement IV and the free energy differences between them is about –2.5 eV/cell.

Therefore, we calculated the structural and electronic properties of $BaMg_xCo_{2-x}Fe_{16}O_{27}$ with different compositions of BMFO (with $x = 2$) using Arrangement I, BCFO (with $x = 0$) using Arrangement III and BMCFO (with $x = 1$) using combinations of the two Arrangements. The results are summarized in Table IV.

TABLE II

Lattice parameters, magnetic moment and free energy of the unit cell of $BaMg_2Fe_{16}O_{27}$

Model	Free energy [ev/cell]	Magnetic moment	a [Å]	c [Å]	c/a
6g-Mg	–621.102	46 μ_B/cell	5.851	32.895	5.622
$4f_3$-Mg	–620.824	46 μ_B/cell	5.877	32.843	5.583
exp. [22]		51.6 μ_B/cell	5.892	32.85	5.575

TABLE III

Lattice parameters, magnetic moment and free energy of the unit cell of $BaCo_2Fe_{16}O_{27}$

Model	Free energy [ev/cell]	Magnetic moment	a [Å]	c [Å]	c/a
6g-Co	–626.325	52 μ_B/cell	5.946	33.201	5.583
$4f_3$-Co	–623.824	52 μ_B/cell	5.959	33.015	5.540
exp. [22]		54.4 μ_B/cell	5.899	32.846	5.568

Since Mg^{2+} cations are found to be in the 6g sites, the substitution of Co^{2+} by Mg^{2+} at $BaMg_xCo_{2-x}Fe_{16}O_{27}$ decreases the distance between layers, which leads to a decrease in lattice parameters. This is due to the fact that the ionic radius of Mg^{2+} (0.65 Å) is smaller than that of Co^{2+} (0.78 Å).

The substitution of the Fe^{2+} in the spin up states (2d, $4f_3$, 6g, 12k) appears to cause a reduction in the magnetization, while the substitution in the spin-down states (4e, $4f_1$, $4f_2$) may lead to an increase in the net magnetization [6]. As we know, Mg^{2+} cation is the diamagnetic cation, and the magnetic moment of Mg^{2+} and Co^{2+} are lower than that of the Fe^{2+} (5.1–5.7 μ_B). Therefore, if the Fe^{2+} in the spin-up states were replaced by Mg^{2+} or Co^{2+}, the net magnetization in upward spin is expected to decrease the total magnetic moment and hence strengthen the magnetization. As we expected the calculated magnetic moments BMFO, BCFO and BMCFO are lower than BFFO and the calculated magnetic moments are somewhat lower than those experimentally determined. This can be due to the fact that our simple model has not considered some of the Mg and Co atoms which might be located in the tetrahedral positions [22].

TABLE IV

Lattice parameters, magnetic moment and free energy of the unit cell of $BaMg_xCo_{2-x}Fe_{16}O_{27}$

		BFFO	BCFO ($x = 0$)	BMCFO ($x = 1$)	BMFO ($x = 2$)
lattice parameters	a [Å]	5.941	5.946	5.901	5.851
	c [Å]	33.30	33.201	33.025	32.895
	c/a	5.605	5.583	5.596	5.622
magnetic moment		56	52	49	46
free energy		–627.614	–626.325	–623.752	–621.102

The total density of states (DOS) for BFFO, BMFO, BMCFO and BCFO is shown in Fig. 3. Energy gap appears in all materials. There is a half metallic peak in the energy gap of BFFO (Fig. 3a), while no peak appears in the energy gap of the other materials BMFO (Fig. 3b), BMCFO (Fig. 3c) and BCFO (Fig. 3d). The substitutions of Mg and Co at the $BaFe_2^{2+}Fe_{16}^{3+}O_{27}$ decrease electrical conductivity and transit it from a half-metal to semiconductor material. Based on our calculations, the BFFO is a weak half-metal, but BMFO, BMCFO and BCFO are semiconductors.

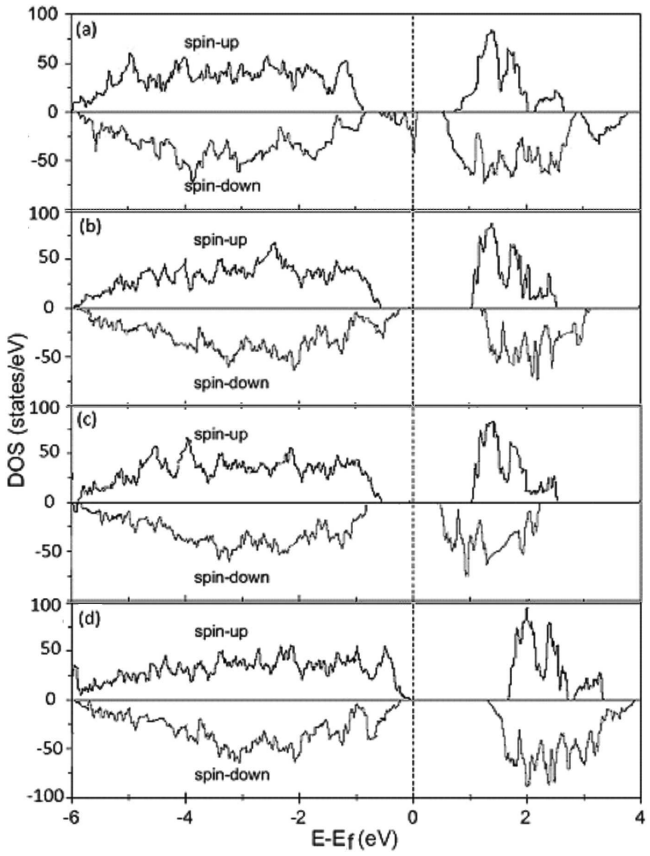

Fig. 3. Total DOS of (a) BFFO and (b) BMFO, (c) BMCFO and (d) BCFO. The spin-up DOS is to be positive, while the spin-down part is set to be negative The spin-up DOS is to be positive, while the spin-down part is set to be negative.

For more detailed consideration, the total DOS was dissolved into the partial DOS of symmetric sites and all contribution to this peak were studied. It turns out that the $3d$ electrons of Fe at 6g sites have most contribution to the BFFO peak and only a small part of the peak comes from oxygen $2p$ electrons at $12k_2$ and $4f_2$ sites, which are located at upper and lower layers nearest to iron 6g sites.

Electronic band structures around energy gap of three materials of BFFO, BMFO, and BCFO are shown in Fig. 4. In all of the materials, the changes of eigenenergy dispersion curves along the direction parallel to c axis (G–A, H–K) are very small, while curves along the directions perpendicular to c axis (A–H, M–G) are rather steep. From the electronic band structure one can finds that the BFFO is a weak half-metal, while BMFO, BMCFO and BCFO are semiconductors.

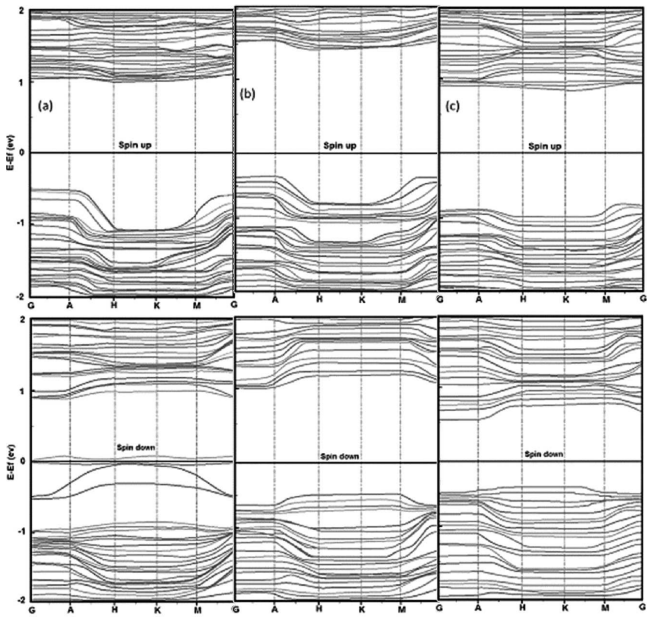

Fig. 4. Energy band structure along the high symmetry directions, G (0 0 0) A (0 0 1/2) H (1/3 1/3 1/2) K (1/3 1/3 0) M (1/2 0 0). Bands (a) for BFFO, (b) for BMCFO, and (c) for BMFO.

The effective mass of the carrier in solid state physics is related with $\partial^2 E/\partial k^2$, where E is eigenenergy at a k point in BZ. Figure 4 indicates that the effective masses of carrier along c axis are much heavier than that perpendicular to c axis. As is known, the electrical conductivity is inversely proportional to the carrier effective mass. Because of the anisotropy of carrier density and the effective mass of carrier, all of the materials experimentally demonstrated to possess a strong anisotropy of electrical resistivities. The electrical resistivity along the c axis relative to perpendicular to c axis is equal to 10^2–10^3. The electrical resistivity in these ferrites is mainly due to hopping electrons between Fe^{2+} and Fe^{3+}. As Co and Mg ions prefer to occupy octahedral sites (6g sites) followed by the migration of some Fe^{3+} ions to tetrahedral sites and converting them into Fe^{2+} ions in order to maintain overall electrical neutrality. As a result Fe^{3+} ions concentration is lowered on octahedral sites: the sites responsible for conduction in ferrites. Therefore, the charge of Fe atom at 6g sites increases to the value level of the other Fe atoms.

It can be considered that Co and Mg doping causes valence state of 6g site to change from mixed valence state to 3+ valence state. Hence, the energy of Fe at 6g states raise up and the corresponding peak in the energy gap moves into the conduction band, and the "doping states"

become extinct and the electric carrier density decreases. All these factors would limit the hopping probability between Fe^{3+} and Fe^{2+} ions thereby enhancing the resistivity. Moreover porosity in the investigated samples has been observed to increase so this prevented the motion of charge carriers and as a result electrical resistivity increases with increasing Co and Mg concentration. This is the main reason why the electrical resistivity of BMFO, BMCFO and BCFO are about 1000 times higher than BFFO.

4. Conclusions

Our calculations on the optimized crystal structure and electronic ground structure have been performed to understand the anisotropy of the electric conductivities in W-type hexagonal ferrites BFFO, BMFO, BMCFO and BCFO. Due to the presence of Fe mixed valence states at 6g sites in BFFO a half-metallic peak appears in the energy gap and it results in an "electrical conductive layer" perpendicular to c axis. Replacement of Fe at 4e and 6g sites of BFFO by Mg and Co, causes the mixed valence states of Fe cations at 6g sites to vanish and the carrier density to be lower. Also, in all materials, effective mass of carrier along c axis is much heavier than that perpendicular to c axis. Therefore, the electrical resistivities of the materials are much different and the electrical resistivities of all materials along c axis are much higher than that perpendicular to c axis. The electrical resistivity increases by increasing Mg and Co contents due to increase in porosity which prevents the hopping of charge carriers.

Acknowledgments

This work has been supported financially by Arak University Research Council (AURC) under the grant number of 90-12646 [90-11-26]. The authors acknowledge from AURC and Grid Computing Group in IPM for the financial support and performing the calculations, respectively. Computer time allocation has been provided by the Grid Computing Group IPM. Also, the authors would like to express their thanks and gratitude to Dr. Y. Taghipour Azar.

References

[1] M. Ahmad, F. Aen, M.U. Islam, S.B. Niazi, M.U. Rana, *Ceram. Int.* **37**, 3691 (2011).

[2] S. Gunes, S.K. Akay, A. Kara, *Acta Phys. Pol. A* **125**, 538 (2014).

[3] M.A. Iqbal, W. Tahir, G. MurtazaRai, N.A. Noor, S. Ali, K.T. Kubra, *Ceram. Int.* **38**, 3757 (2012).

[4] M.A. Ahmed, N. Okasha, R.M. Kershi, *Physica B* **405**, 3223 (2010).

[5] M.J. Iqbal, R. A. Khan, S. Mizukami, T. Miyazaki, *J. Magn. Magn. Mater.* **323**, 2137 (2011).

[6] Y. Wu, Y. Huang, L. Niu, Y. Zhang, Y. Li, X. Wang, *J. Magn. Magn. Mater.* **324**, 616 (2012).

[7] D.M. Hemeda, A. Al-Sharif, O.M. Hemeda, *J. Magn. Magn. Mater.* **315**, L1 (2007).

[8] S.M. Attia, A.M. Abo El Ata, D. El Kony, *J. Magn. Magn. Mater.* **270**, 142 (2004).

[9] C.M. Fang, F. Kools, R. Metselaar, G. de With, R.A. de Groot, *J. Phys. Condens. Matter.* **15**, 6229 (2003).

[10] M. Feng, B. Shao, J. Wu, X. Zuo, *J. Appl. Phys.* **113**, 17D909 (2013).

[11] L.S.I. Liyanage, S. Kim, Y.-K. Hong, J.-H. Park, S.C. Erwin, S.-G. Kim, *J. Magn. Magn. Mater.* **348**, 75 (2013).

[12] C.H. Ri, L. Li, Y. Qi, *J. Magn. Magn. Mater.* **324**, 1498 (2012).

[13] S. Baroni, P. Giannozzi, A. Testa, *Phys. Rev. Lett.* **58**, 1861 (1987).

[14] K. Laasonen, A. Pasquarello, R. Car, C. Lee, D. Vanderbilt, *Phys. Rev. B* **47**, 10142 (1993).

[15] J.P. Perdew, K. Burke, M. Ernzerhof, *Phys. Rev. Lett.* **77**, 3865 (1996).

[16] W. Kohn, L.J. Sham, *Phys. Rev.* **140**, A1133 (1965).

[17] P. Hohenberg, W. Kohn, *Phys. Rev.* **136**, B864 (1964).

[18] P. Giannozzi S. Baroni, N. Bonini, M. Calandra, R. Car, C. Cavazzoni, D. Ceresoli, G.L. Chiarotti, M. Cococcioni, I. Dabo, A. Dal Corso, S. de Gironcoli, S. Fabris, G. Fratesi, R. Gebauer, U. Gerstmann, C. Gougoussis, A. Kokalj, M. Lazzeri, L. Martin-Samos, N. Marzari, F. Mauri, R. Mazzarello, S. Paolini, A. Pasquarello, L. Paulatto, C. Sbraccia, S. Scandolo, G. Sclauzero, A.P. Seitsonen, A. Smogunov, P. Umari, R.M. Wentzcovitch, *J. Phys. Condens. Matter* **21**, 395502 (2009) [www.quantum-espresso.org].

[19] H.J. Monkhorst, J.D. Pack, *Phys. Rev. B* **13**, 5188 (1976).

[20] E.W. Gorter, in: *Proc. IEE104B* **104**(5S), 255 (1957).

[21] M.A. Ahmed, N. Okasha, M. Oaf, R.M. Kershi, *J. Magn. Magn. Mater.* **314**, 128 (2007).

[22] A. Collomb, P. Wolfers, X. Obradors, *J. Magn. Magn. Mater.* **62**, 57 (1986).

[23] A. Collomb, O. Abdelkader, P. Wolfers, J.C. Guitel, *J. Magn. Magn. Mater.* **58**, 247 (1986).